CROATICA CHEMICA ACTA CCACAA 64 (2) 111–127 (1991)

YU ISSN 0011-1643
UDC 546.72
CCA-1984

Original Scientific Paper

Impedance of $Fe_{80}B_{20}$ Glassy Alloy in Sulphuric Acid

D. Hodko, K. Kvastek, V. Horvat and V. Pravdić*

Center for Marine Research and Department of Physical Chemistry, Ruđer Bošković Institute, P.O.Box 1016, 41001 Zagreb, Croatia, Yugoslavia

Received March 18, 1991

Experimental investigations of corrosion behavior of glassy metal $Fe_{80}B_{20}$ in 1.0 mol dm^{-3} H_2SO_4 are described. Results are presented on voltametric and impedance measurements in three distinct anodic potential ranges. Two relaxation processes have been observed and identified: i) a kinetically controlled interfacial charge transfer mediated by adsorption of some intermediate species in the active dissolution range; ii) the same process, but with a blocking effect due to adsorption of the passivating species in the passivation or transition range; and iii) ion migration in a high electric field within the passive layer with adsorption of surface states in the passive range. Using a general impedance of the resistance, the measured impedances have been characterized in terms of parameters of compatible equivalent circuits.

INTRODUCTION

Ever since the time when it was reported that some amorphous metal-metalloid (glassy) alloys were better corrosion-resistant materials than crystalline alloys, containing a similar amount of elements, the corrosion behavior and passivation of glassy alloys have been the subject of numerous investigations.[1-4] The glassy alloys are supposedly in state which is free of defects associated with the crystalline state and, therefore, can be regarded as ideally homogeneous solution alloys. In a series of papers, Heusler and Huerta[5-7] have shown, that the rate of dissolution of a glassy alloy is greater than the rate of dissolution of a crystalline alloy of the same composition, which has been related to the lesser activity of the components in the crystalline state. On the other hand, the extremely high corrosion resistance, observed particularly if Cr was present in the glassy alloy[2,8-10], led to the conclusion about the crucial influence of chemical composition on the corrosion properties of glassy alloys. Besides the presence of Cr, the presence of the metalloid P was assumed to be beneficial for the purpose of stimulating rapid initial dissolution of the surface and rapid development of a

* To whom correspondence should be addressed

corrosion resistant passive film. However, the role of the surface structure, and of the metalloid present in the glassy alloy, is not yet clear, particularly if we take into account the results obtained for the simple binary alloys such as $Fe_{80}X_{20}$ (X=B,Si,C,P). Electrochemical studies of glassy $Fe_{80}B_{20}$ alloys in acidified sulphate solutions have not shown polarization behavior noticeably different from that of pure crystalline Fe in the active[11-14] and passivation or transition regions[11] of anodic potentials. Furthermore, in the passive region of $Fe_{80}B_{20}$, much higher passive current densities were observed.[11] Higher stability of the passive layer, but lower dissolution rates in the active and passive regions, were observed if B was substituted by other metalloids, particularly by phosphorus.[13] However, for both alloys, the properties of the passive layer are degraded if compared with pure crystalline iron. The same was observed if passive layers were formed in borate buffer solutions.[15,16]

Since all these results were obtained by the electrochemical *dc* measurements, it was considered essential to carry out studies of corrosion behavior using the *ac* impedance technique, particularly because of its ability to detect relaxation processes that cover a wide range of relaxation times.[17,18] Emphasis is placed on detailed analysis of the frequency impedance spectrum in order to identify and characterize the processes that occur on $Fe_{80}B_{20}$ in 1.0 mol dm^{-3} H_2SO_4 (pH=0.12) in different regions of anodic potentials. Additional data were expected to elucidate the differences in impedance data between the pure crystalline Fe and the $Fe_{80}B_{20}$ glassy alloy in order to understand the surface reactions involving boron.

EXPERIMENTAL

Materials and Electrodes

The amorphous $Fe_{80}B_{20}$ (numbers indicate at. %) working electrodes were ribbons (25 μm thickness and 2 mm width), produced by melt spinning on a rotating cylinder. The shiny side of ribbons (0.07–0.15 cm^2 of geometric area) was exposed to the electrolyte solution. The electrical contact was made by pressing the ribbon to a Cu-cylinder with fibreglass screws. The remaining parts of the ribbons were covered with sealed epoxy resin and were mounted to fibreglass holders.

Before the experiments, the electrodes were cleaned with acetone and washed with quadruply distilled water.

The electrolyte solution was 1.0 mol dm^{-3} H_2SO_4, prepared from analytical purity grade chemical (Merck, W. Germany) and quadruply distilled water. Prior to experiments, the electrolyte in the cell was purged with purified nitrogen. All measurements were made at room temperature (296±2 K). A three-electrode conventional electrochemical cell was used, with Pt-counter electrode of large surface area, separated from the main cell compartment by a glass diaphragm. Due to the very high conductance of the electrolyte used, there was no need for close electrode spacing.

A saturated calomel electrode (SCE) (K 401, Radiometer, Denmark), situated in a separate compartment with a glass frit and a Haber-Luggin capillary about 1 mm from the electrode surface, served as the reference electrode and all potentials are given with respect to this electrode.

Polarization Measurements

The steady-state polarization curve was obtained through point by point measurements, starting from –0.450 V, with potentiostatic steps of 25 mV every five minutes. This was sufficient to obtain steady-state currents in the whole investigated range, except at potentials lower than –0.400 V where extended time for stabilization was needed.

Impedance Measurements

The impedance measurements were made by using the Frequency Response Analyser (Model 1250) and the Electrochemical Interface (Model 1286), both of Schlumberger-Solartron, U.K., integrated with a Hewlett-Packard computer system (Model 9816).

In the preliminary experiments, the linearity of the measured impedance was tested (both in the active and passive regions) by the perturbing signal of 1, 5 and 10 mV rms. To achieve linearity and to obtain a satisfactory signal to noise ratio, the chosen amplitude of the perturbing signal in the experiments presented here was 5 mV rms.

The existence of possible deviations of the cell response at high frequencies due to the ohmic resistance and stray capacitances of the capillary was tested by a low impedance platinum probe connected via a 5 μF capacitance in parallel with the reference electrode.[19] No change in the measured data was observed.

The cell impedances were measured at the potential points adjusted in the same way as the polarization curve was obtained, and when steady state currents were reached. Some impedance measurements were performed at passive films formed by anodic oxidation in 1.0 mol dm^{-3} H_2SO_4 at +1.40V for 20 minutes and then switched and stabilized at the desired potential.

To compromise the required precision and the required time for data acquisition, the following two procedures were used. At potentials between –0.450 V and +0.050 V, the frequency range between 20,000 and 1 Hz was covered by equidistant spacing of 15 points within a log frequency decade, taking measurements of 5 cycles for each frequency, with 1 cycle delay for stabilization. Precise measurements at frequencies lower than 1 Hz were not possible because of dissolution of the electrode material in the active dissolution range, and because of frequent appearance of spontaneous current oscillations in the passivation or transition range. At potentials above +0.050 V, the measurements were improved by the use of 1 s delays for stabilization at each frequency, and by extending the low frequency limit to 0.5 Hz.

RESULTS AND DISCUSSION

The Polarization Curve

Figure 1 shows the steady-state anodic polarization curve of a $Fe_{80}B_{20}$ stationary electrode in 1.0 mol dm^{-3} H_2SO_4. The active dissolution range stretches between E_{corr} (–0.480 V) and E_{max} (–0.250 V). The passivation range is between –0.250 V and +0.275 V. At higher anodic potentials, stable and potential independent currents were observed. Beyond +1.30 V, the increase of current indicates the beginning of the oxygen evolution reaction. Thus, the full passive range could be explored over the potential range of about 1 V.

The reproducibility of the polarization curves obtained after several runs of experiments, performed on a number of electrodes, was perfect in the active and passive ranges, and less reproducible in the passivation or transition range. Thus, reproducible passive current densities of 0.34–0.42 mA/cm^2 are always obtained, while current densities at E_{max} were between 90 and 200 mA/cm^2. Among the few papers on this subject in the literature, there is one in which a polarization curve is obtained in sulphuric acid-sodium sulphate solutions at pH = 1.0, with nearly equal E_{corr}, potential ranges of active dissolution and passivation, current densities, and full passive range of about 0.8 V.[11] In comparison with data obtained on pure, polycrystalline Fe/pH=0[20,21], the passive current over one order of magnitude higher is the most prominent difference.

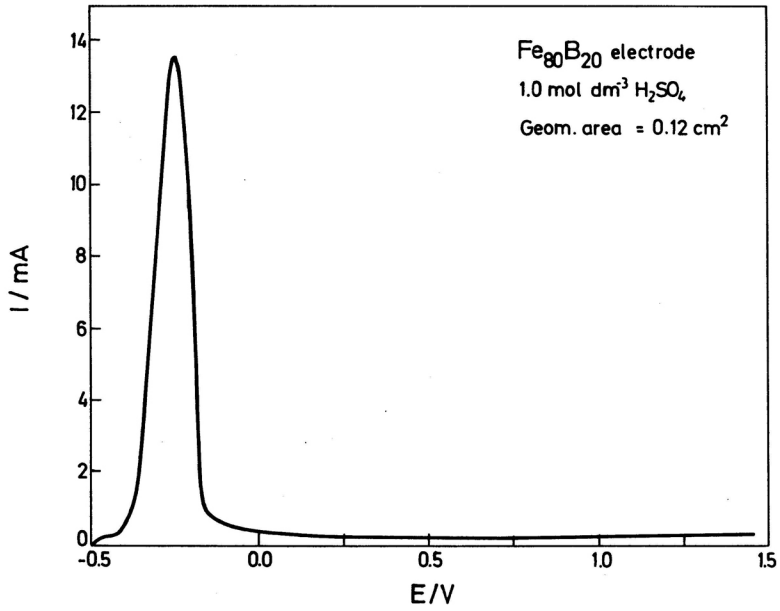

Figure 1. Steady-state anodic polarization curve for the $Fe_{80}B_{20}$ electrode in 1.0 mol dm^{-3} H_2SO_4.

Electrode Impedance

(i) The Active Dissolution Range

In Figure 2, the electrode impedances are shown as $-Z''$ *vs.* Z' dependences. The values were obtained from the measured cell impedances after correction for electrolyte resistances. These were obtained as high frequency intercepts of measured impedances with the real axis.[18] In all the ranges of potential studied here, the mean value of the electrolyte resistance was 3.0±0.3 ohms.

From Figure 2, it appears that in the active dissolution range at –0.450 V, only one capacitative loop is observed. At potentials between –0.425 V and –0.325 V, the capacitative loops at higher frequencies are followed by inductive loops at lower frequencies.

The obtained frequency dispersion of the measured impedance could be interpreted as the noninstantaneous potential dependence of resistance, R, due to the existence of one another state variable, X, varying with potential. In such a case, the electrode admittance Y can be defined as[20–23]:

$$Y = iwC + 1/R + A/(iw+B) \quad (1)$$

where i is an imaginary unit, w is angular frequency, C is a potential dependent capacitance related to relaxation at high frequencies, while A and B are potential dependent terms related to relaxation at low frequencies. In dependence on the sign of parameter A, the impedance plane display will exhibit inductive ($A > 0$) or capacitative ($A < 0$) shape.

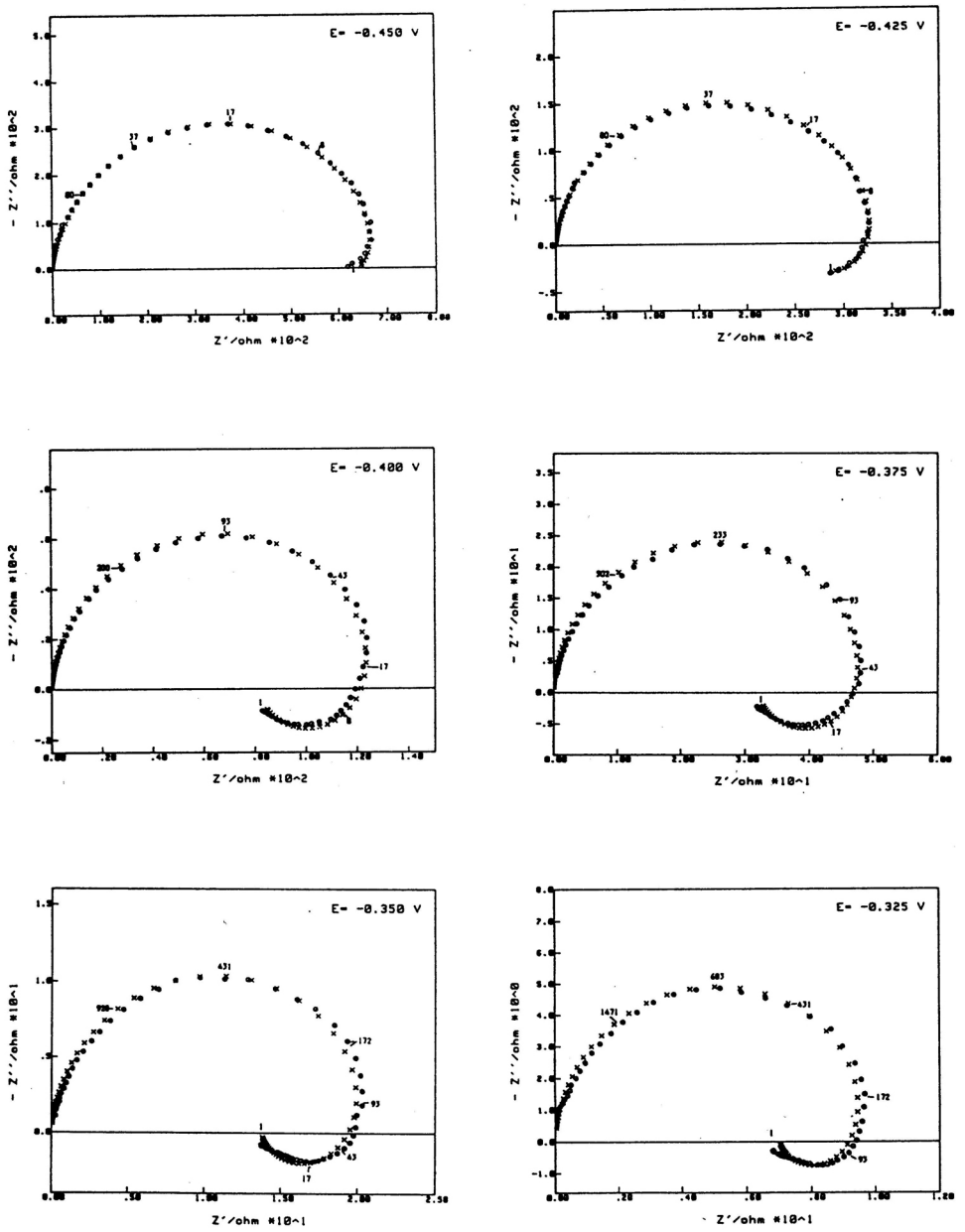

Figure 2. Complex plane impedance plot for the $Fe_{80}B_{20}$ electrode in 1.0 mol dm^{-3} at selected potentials in the active range. Numbers indicate frequencies in Hz. Measured data are represented by (o), CNLS fits obtained using eqns. (2) and (6-7) are represented by (x).

In the active dissolution range, the capacitative relaxation process observed at high frequencies is usually[17,20], attributed to the charge transfer resistance R_t due to the kinetically controlled electrochemical oxidation of Me with a non-faradic contribution from the double-layer capacitance C_{dl}. The inductive (or capacitative) behavior at low frequencies is attributed to the relaxation of one (or more) potential dependent variables related to the state of the surface. This can be the fractional surface coverage, X, either of the adsorbed species or of the active sites blocked.

If data are analyzed in terms of equivalent circuits, the components should be interpreted as phenomena exhibiting the same frequency behavior as the system. However, the choice between the circuits lies in the fact that the »natural« circuit is the one with positive components.[20,22,23] Thus, if the inductive behavior at low frequencies is observed, the total electrode admittance can be analyzed in terms of the charge transfer resistance R_t in parallel with C_{dl} and both in parallel with the series connection of resistance R_o and inductivity L, according to:

$$Y = iwC_{dl} + 1/R_t + 1/(R_0 + iwL) \tag{2}$$

Here, the polarization resistance, R_p, defined as the zero frequency limit of the impedance is equal to:

$$R_p = R_0R_t/(R_0 + R_t) \tag{3}$$

If capacitative behavior at low frequencies is observed, the total electrode admittance could be defined in terms of parallel R_aC_a connections in series with R_t and all in parallel with C_{dl}, as:

$$Y = iwC_{dl} + 1/R_t + (C_aR_t^2)^{-1}/[(C_aR_t)^{-1} + (C_aR_a)^{-1} + iw] \tag{4}$$

Here, R_p is defined according to:

$$R_p = R_t + R_a \tag{5}$$

The equivalent circuits described by eqns. (2) and (4) are drawn in Figure 3. Since eqns. (2) and (4) are in fact only two forms of eqn. (1), equivalent circuits in Figure 3 correspond to eqn. (1) with $A > 0$ (Figure 3a) and $A < 0$ (Figure 3b) if all circuit

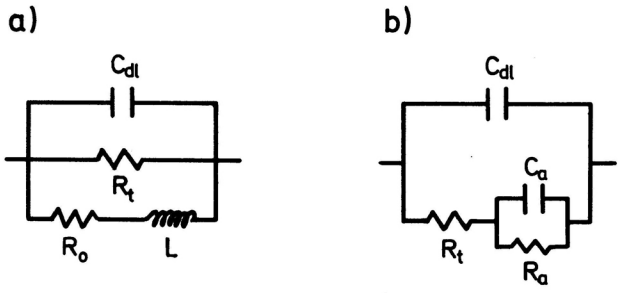

Figure 3. Equivalent circuits described by: a) eqn. (2), b) eqn. (4).

elements are chosen to be positive. In both cases, R_t is associated with the charge transfer part of the current response which occurs without a change in X. The branch containing series R_oL (Figure 3a) or the part of the branch containing parallel R_aC_A (Figure 3b) is associated with the part of the current response which occurs as X changes. Inductance L has similar significance as capacitance C_a and both are in relation with adsorption pseudocapacitance.[22] The phase delay of surface relaxation is modelled by a combination of these L and C_a values with resistances R_o and R_a. In all, the phase delay is, consequently, not $\pi/2$.

Turning back to Figure 2, where only one capacitative loop is observed, it follows that for –0.450 V, there is no surface state relaxation process in the frequency range down to 1 Hz. For anodic potentials between –0.425V and –0.325V, inductive behavior is observed at low frequencies, and the electrode admittance can be analyzed using eqns. (2-3). The values of the frequency independent parameters which characterize each loop, together with the corresponding characteristic frequencies of relaxation, are in dependence on the anodic potential, summarized in Tables I and II.

The parameter values are estimated as follows: R_t values are obtained graphically from the zero-frequency real axis intercepts of the »least square fitting« of high-frequency circles. For the high frequency circle at each potential, the frequency of the top of the circle, f_{max1}, is determined as the slope of Z' *vs.* wZ'', a straight line obtained in the narrow frequency range around the maximal value.[18] C_{dl} values are calculated from R_t and f_{max1}. In addition, the departure from the ideal semicircle behavior is given in Table I as tan ϕ_1, ϕ_1 being the angle between the real axis and the radius vector

TABLE I

Characteristic impedance parameters from high frequency (capacitative) loops of $Fe_{80}B_{20}$/1.0 mol dm^{-3} H_2SO_4 in dependence on anodic potentials in the active dissolution range. The geom. area = 0.10 cm^2

E/V	R_t/Ω	f_{max1}/Hz	C_{dl}/μF	tan ϕ_1
–0.450	710.3	18	12.4	0.14
–0.425	336.2	34	13.9	0.12
–0.400	131.6	92	13.1	0.08
–0.375	49.6	240	13.4	0.05
–0.350	21.2	440	17.0	0.04
–0.325	10.8	700	21.0	0.07

TABLE II

Characteristic impedance parameters from low frequency (inductive) loops of $Fe_{80}B_{20}$/1.0 mol dm^{-3} H_2SO_4 in dependence on anodic potentials in the active dissolution range. The geom. area = 0.10 cm^2

E/V	R_p/Ω	f_{max2}/Hz	R_o/Ω	L/H	tan ϕ_2
–0.450	710.3	–	–	–	–
–0.425	246.1	1	918.3	146.2	0.23
–0.400	80.4	3.2	206.7	10.3	0.37
–0.375	30.5	8.5	79.2	1.6	0.43
–0.350	13.1	17.1	34.3	0.3	0.44
–0.325	6.5	27.2	16.3	0.1	0.41

to point R_t. Polarization resistances R_p are determined as zero-frequency intercepts of the best fitting inductive circles. From R_p and R_t, R_o values are calculated by the use of eqn. (3), while f_{max2} and tan ϕ_2 are determined in the same way as f_{max1} and tan ϕ_1. Finally, L values are calculated from R_o and f_{max2}. The appearance of depressed circles is usually attributed to the inhomogeneities of the solid phase, and in the curve fitting procedure it could be accounted for by the use of constant phase elements (*CPE*) instead of capacitance and inductance according to[24-26]:

$$Z_{CPE}(w) = 1/K_{CPE}(iw)^{\alpha} \tag{6}$$

$$Z_{CPE}(w) = L_{CPE}(iw)^{\beta} \tag{7}$$

where frequency independent constants K_{CPE} and L_{CPE} are equal to C_{dl} and L if α and β are equal to 1. Parameters α and β define the frequency dependence and phase angle of the corresponding impedance, being in relation with ϕ_1 and ϕ_2 through[24,25]:

$$\varphi_1 = (1-\alpha)\,\pi/2 \qquad \varphi_2 = (1-\beta)\,\pi/2 \tag{8}$$

In Table III, the impedance parameters R_t, K_{CPE}, α, R_o, L_{CPE} and β, evaluated by the complex non-linear least square fit (CNLS) procedure using eqns. (2) and (6-7), are listed. Unity-weighting, and data in Tables I and II were used as initial values. The average relative errors of the overall fits reported in this paper were lass than 10%.

TABLE III

Characteristic impedance parameters for $Fe_{80}B_{20}$ in 1.0 mol dm^{-3} H_2SO_4 in dependence on anodic potential in the active dissolution range. Data are obtained by the curve fitting procedure, using eqns. (2) and (6-7).

E/V	R_t/Ω	$\frac{K_{CPE} \times 10^6}{\Omega^{-1}s^{\alpha}}$	α	R_o/Ω	$L_{CPE}/\Omega s^{\beta}$	β
–0.450	715	19.1	0.91	5000	600	0.95
–0.425	346	22.0	0.91	918	200	0.90
–0.400	137	17.8	0.95	195	13.3	0.83
–0.375	51	16.9	0.97	85	4.0	0.82
–0.350	23	24.6	0.96	34	0.5	0.80
–0.325	10.8	35.5	0.96	20	0.2	0.81

After comparing the data in Table I-III, it appeared that there is a good agreement between the corresponding parameter values, even for the potential of –0.450 V, which means that all the experimental data are well fitted by eqn. (2) involving CPE. This is also demonstrated by the close agreement of experimental and fitted impedance curves drawn in Figure 2. From data in Tables I-III it appears that, in the active dissolution range, there is a considerable decrease of all resistance values. This is in full agreement with the sharp increase of the faradaic current given in Figure 1. Relatively high values of R_t and R_p at low anodic potential may indicate hydrogen adsorption which hinders the metal dissolution process. It is supported by the slow attainment of steady-state at potentials near the open circuit corrosion potential. At higher anodic potentials, the resistance values are rather low, indicating vigorous corrosion of $Fe_{80}B_{20}$. De-

creases of resistance values are accompanied by a marked increase of f_{max} values. C_{dl} values are nearly constant and increase slightly after –0.350V.

The values of tan ϕ_1 (Table I) and α (Table III) indicate a possibly quite homogeneous structure of $Fe_{80}B_{20}$. Somewhat higher values of tan ϕ_2 (Table II) and lower values of β (Table III) indicate several relaxation processes, becoming more prominent as the anodic potential increases.

All the data obtained for $Fe_{80}B_{20}$ indicate a rise of the overall faradaic reaction rate with potential at constant surface coverage, and with surface coverage at constant potential. It may be stated that the overall process is a kinetically controlled charge transfer going through adsorption of some surface species, which is in general agreement with data and conclusions presented for pure, polycrystalline Fe-sulphate systems in pH 0-5.[20,25,27-35] It means that $Fe_{80}B_{20}$ dissolves through mechanism similar to that for pure Fe. The influence of the presence of B is evident only through somewhat higher C_{dl} and L values, which together with near the same R values leads to higher f_{max} of both relaxations. Using the geometrical area of the electrode, C_{dl} values of 125–210 $\mu F/cm^2$ were obtained. These results indicate that, possibly, a parallel anodic dissolution of B increases the faradaic pseudocapacitance. The values are higher than the C_{dl} values (50–100 $\mu F/cm^2$) obtained in the same manner for pure Fe[31,34,35].

(ii) The Passivation (or Transition) Range

A change in the reaction path is indicated at –0.300V, where capacitative behavior at low frequencies is observed (Figure 4A). Obviously, $R_p > R_t$ as predicted by eqn. (5). Furthermore, low values of f_{max2} and R_o indicate high values of C_a.

At more anodic potentials, the impedance plane display is changed. At potential of –0.250V, *ie.* at the maximum of the polarization curve in Figure 1, the process at the lower end of frequencies becomes the dominant impedance. This is obvious from Figure 4A, where the vertical line denotes a pure capacitance. At the potential of –0.225 V, the low frequency capacitance curve bends to the negative real-axis interception (Figure 4A). This is in agreement with the equivalent circuit defined by eqn. (4) and drawn in Figure 3b, with R_a of infinite or negative value. According to eqn. (5), this leads to infinite or negative R_p values, and is in agreement with the infinite, or negative slope of the steady-state polarization curve in Figure 1.

This kind of behavior is characteristic of a passivation process, when R_a can be positive, infinite, or negative.[20,22] The rough estimates of characteristic parameter values for potential points around the maximum of the polarization curve are listed in Table IV, where C_a and R_a values were estimated from impedance at low frequencies. Impedances calculated according to eqns. (4) and (6), with parameter values manually adjusted to give the closest agreement between the calculated and experimental data, are drawn in Figure 4B. The characteristic parameter values are listed in Table V, where K_{aCPE} and α_2 denote parameters of *CPE* impedance which replaces ideal C_a.

Somewhat better description of phenomena at potentials of –0.300 V and –0.250 V is obtained if eqn. (4) is extended to the one derived for the case where two surface state variables X are involved in the overall electrode process (eqn. 15 of ref.[23]). In such a case, there will be three time constants, as it was already observed in the impedance plane display drawn in Figure 4A. Using the cited equation, the inductive behavior at intermediate frequencies, observed at potentials –0.300 V and –0.250 V, is accounted for (cf. Figure 4B).

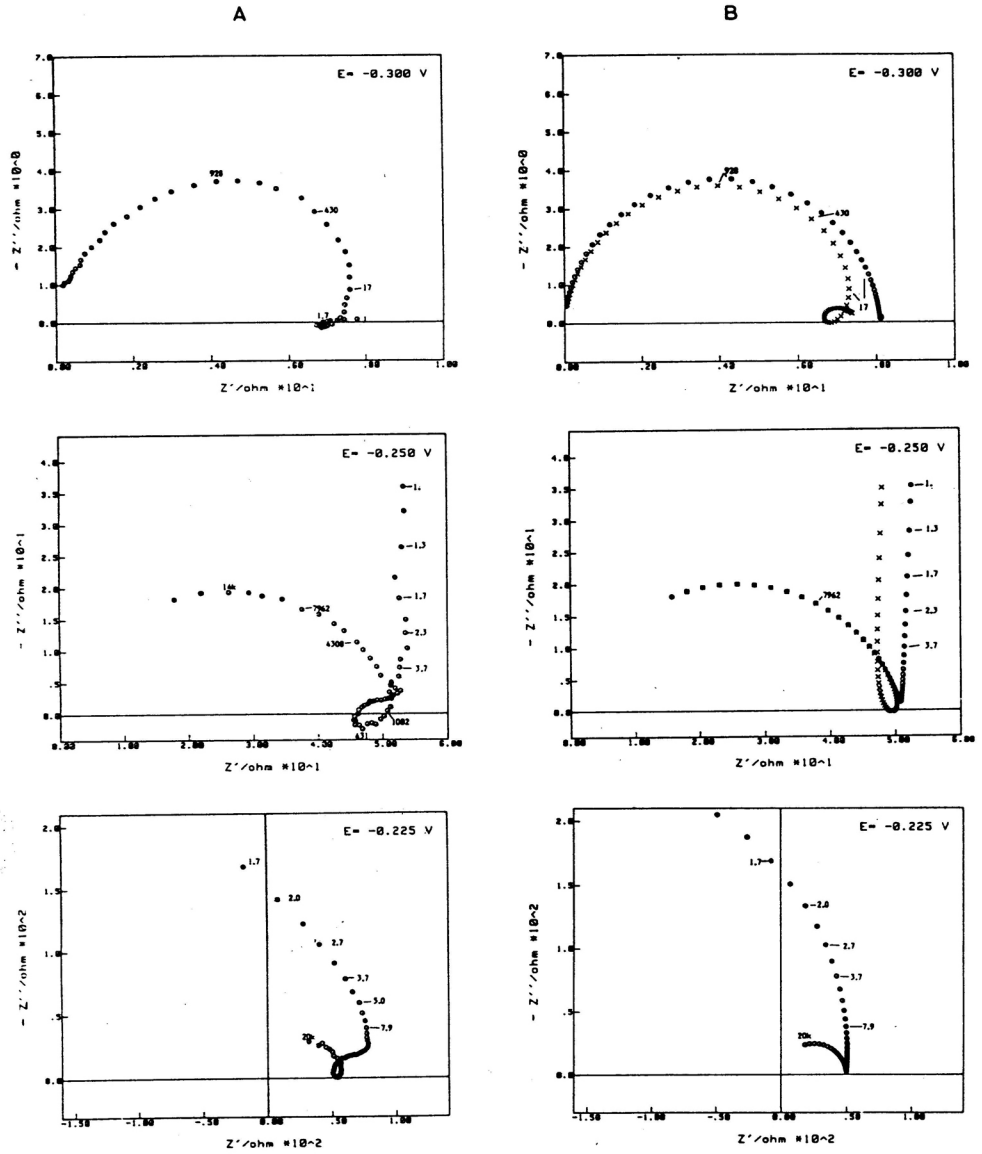

Figure 4. Complex plane impedance plot for the $Fe_{80}B_{20}$ electrode in 1.0 mol dm^{-3} H_2SO_4 at –0.300 V, –0.250 V and –0.225 V *vs.* SCE. Numbers indicate frequencies in Hz.

A) Measured data are represented by (o).

B) Impedances calculated using eqns. (4) and (6) and data in Table V are represented by (o). Impedances calculated using eqns. (15) of ref.[23] and (6-7) are represented by (x). Data for –0.300 V: R_t = 8 Ω; K_{CPE} = 38 x 10^{-6} $\Omega^{-1}s^{\alpha_1}$; α_1 = 0.90; R_a = 1.5 Ω; K_{aCPE} = 0.04 $\Omega^{-1}s^{\alpha_2}$; α_2 = 0.70; R_o = 25 Ω; L_{CPE} = 0.1 Ωs^{β}; β = 0.90. Data for –0.250 V: R_t = 51 Ω; K_{CPE} = 1.6 x 10^{-6} $\Omega^{-1}s^{\alpha_1}$; α_1 = 0.85; R_a = 10^5 Ω; K_{aCPE} = 4.76 x 10^{-4} $\Omega^{-1}s^{\alpha_2}$; α_2 = 0.97; R_o = 500 Ω; L_{CPE} = 10 Ωs^{β}; β = 0.81.

TABLE IV

Characteristic impedance parameters for $Fe_{80}B_{20}$ in 1.0 mol dm^{-3} H_2SO_4 at anodic potentials around the maximum of the polarization curve.. The geom. area = 0.10 cm^2

E/V	R_t/Ω	f_{max1}/Hz	$C_{dl}/\mu F$	$C_a/\mu F$	R_a/Ω
−0.300	8.1	900	21.8	>4600	>0
−0.250	51	15000	0.2	~4600	∞
−0.225	46	20000	0.2	<4600	<0

TABLE V

Characteristic impedance parameters for $Fe_{80}B_{20}$ in 1.0 mol dm^{-3} H_2SO_4 at anodic potentials around the maximum of the polarization curve. Data are obtained from calculations, using eqns. (4), and (6), which give the closest agreement with experimental data.

E/V	R_t/Ω	$\frac{K_{CPE} \times 10^6}{\Omega^{-1}s^{\alpha 1}}$	α_1	$\frac{K_{aCPE} \times 10^6}{\Omega^{-1}s^{\alpha 2}}$	R_a/Ω	α_2
−0.300	8.1	29.0	0.96	2×10^6	40	0.90
−0.250	51	0.6	0.85	4761	1×10^5	0.97
−0.225	50	0.3	0.95	555	−450	0.98

The results can be interpreted as follows: At the potential of −0.300 V, there is a strong dissolution, indicated by low values of R_t. The surface coverage with passivation species (other than those adsorbed) is low, as indicated by low R_a and high C_a. At the point of the maximum of the polarization curve (−0.250 V), the surface coverage is large, as indicated by infinite R_a and C_a lower than previously. The charge transfer is apparently hindered *ie.* it is suppressed on the minor part of the electrode surface that is not yet covered. At −0.225 V, at the descending branch of the polarization curve, the surface coverage is almost unity, C_a is relatively small, while R_a is large and negative.

At more anodic potentials (−0.200 V to +0.025 V), the impedance plane display shows the frequency dependent rotation through all four quadrants in the complex plane terminating at the real axis at positive values. The passivation is very rapid with film instability phenomena, and the steady state cannot be properly controlled. At potentials between +0.050 V and +0.275 V, more stable and reproducible currents are obtained, with the high frequency loop followed by more capacitative loops. The formation of passive layer probably proceeds through various different surface species.

(iii) The Passive Range

From Figure 1, it follows that the passive state for $Fe_{80}B_{20}$ is realized beyond +0.050 Vm but the full passive range, with constant and potential independent passive current, is attained for potentials greater than +0.275 V. In Figure 5, the impedances at potentials +0.300 V and +0.325 V are shown.

The same, but with apparently less scatter of measured data, is obtained for the passive layer previously formed by 20 min of potentiostatic oxidation at +1.40 V, and measured at +1.30 V, +1.20 V, +1.10 V and +1.00 V (Figure 6).

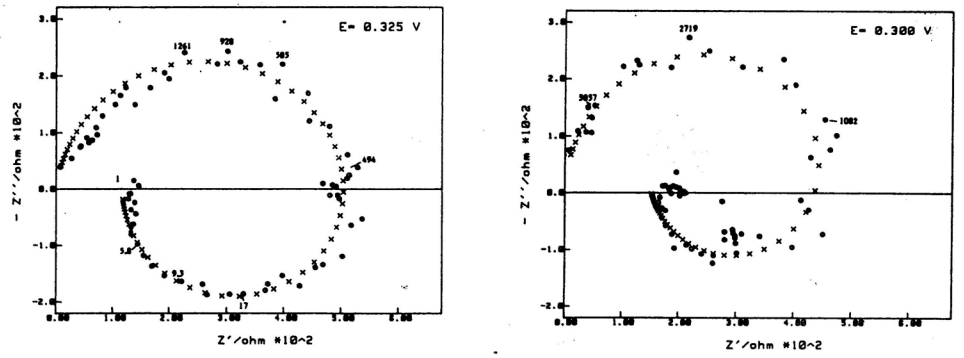

Figure 5. Complex plane impedance plot for the $Fe_{80}B_{20}$ electrode in 1.0 mol dm^{-3} H_2SO_4 at potentials +0.300 V and +0.325 V *vs.* SCE. Numbers indicate frequencies in Hz. Measured data are represented by (o), impedances calculated using eqns. (2) and (6-7) and data in Tables VI and VII are represented by (x).

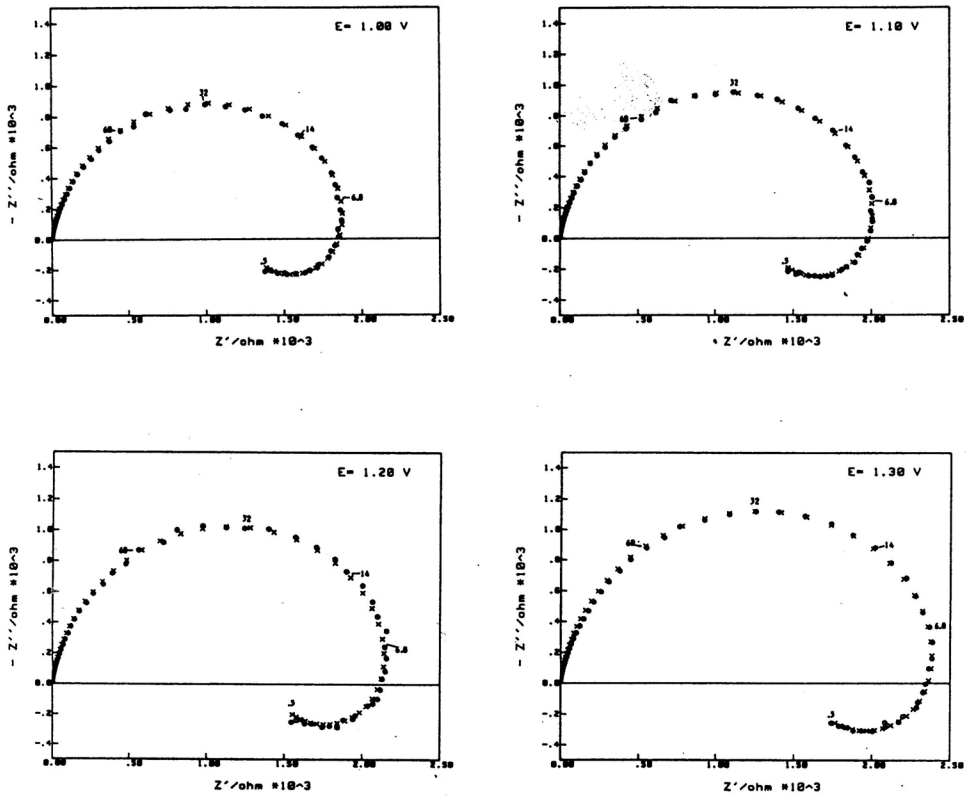

Figure 6. Complex plane impedance plot for the $Fe_{80}B_{20}$ electrode passivated in 1.0 mol dm^{-3} H_2SO_4 by potentiostatic oxidation at +1.40 V *vs.* SCE and measured at selected potentials in the passive range. Numbers indicate frequencies in Hz. Measured data are represented by (o), CNLS fits obtained using eqns. (2) and (6-7) are represented by x.

From Figures 5 and 6, it appears that as in the case of electrode dissolution, the total process is delayed. There is one additional slow process, manifested by an inductive loop at low frequencies. Therefore, eqn. (1) should be used in further analysis of the impedance data. Here, $R_{HF}C_{HF}$, the parallel combination at high frequencies, is regarded as a property of the electrode without modulation of the slower process, described by the third term in eqn. (1). Assessments of the parameter values were made as in the case of dissolution (Tables I and II), and are listed in Tables VI and VII. The values of R_{HF} and C_{HF} are obtained in the same way as R_t and C_{dl}.

TABLE VI

Characteristic impedance parameters from high frequency (capacitative) loops of $Fe_{80}B_{20}$/1.0 mol dm^{-3} H_2SO_4 in dependence on the anodic potential in the passive range.
A) The geom. area = 0.10 cm^2
B) The geom. area = 0.15 cm^2

	E/V	R_{HF}/Ω	f_{max1}/Hz	$C_{HF}/\mu F$	tan ϕ_1
A)	+0.300	450	2500	0.14	0.04
	+0.325	486	1082	0.30	0.14
B)	+1.00	2005	29.3	2.71	0.14
	+1.10	2160	31.4	2.35	0.13
	+1.20	2312	32.8	2.10	0.12
	+1.30	2455	33.8	1.92	0.11

TABLE VII

Characteristic impedance parameters from low frequency (inductive) loops of $Fe_{80}B_{20}$/1.0 mol dm^{-3} H_2SO_4 in dependence on the anodic potential in the passive range.
A) The geom. area = 0.10 cm^2
B) The geom. area = 0.15 cm^2

	E/V	R_p/Ω	f_{max2}/Hz	R_0/Ω	L/H	tan f_2
A)	+0.300	150	300	225	0.1	0.4
	+0.325	100	15	125	1.3	0.1
B)	+1.00	1229	0.69	3175	733	0.28
	+1.10	1328	0.88	3448	624	0.24
	+1.20	1397	0.74	3530	760	0.27
	+1.30	1560	0.75	4279	909	0.25

In Table VIII the characteristic impedance parameter values, obtained by curve fitting procedure using eqns. (2) and (6-7), are listed. Data for potentials of +0.300V and +0.325V are estimated from calculations, with parameter values manually modified after each calculation to give the closest agreement with experimental data. Data for higher potentials are obtained after the CNLS fitting procedure. Unity-weighting and data in Tables VI and VII were used as initial values.

Comparing data in Tables VI-VIII with those in Tables I-III, it appears that much higher impedances (higher real and higher imaginary components) are obtained for passive $Fe_{80}B_{20}$ than for the active dissolution range. The potential dependence of the impedance parameter values is reversed. All resistance values increase with anodic

TABLE VIII

Characteristic impedance parameters for $Fe_{80}B_{20}$/1.0 mol dm^{-3} H_2SO_4 in dependence on anodic potential in the passive range. Data are obtained by curve fitting procedure, using eqns. (2) and (6-7).

E/V	R_{HF}/Ω	$\frac{K_{CPE} \times 10^6}{\Omega^{-1}s^{\alpha}}$	α	R_o/Ω	$L/\Omega s^{\beta}$	β
+0.300	550	0.19	0.97	210	0.8	0.82
+0.325	520	0.62	0.91	150	5.0	0.98
+1.00	2100	4.25	0.91	3000	700	0.80
+1.10	2250	3.73	0.91	3200	700	0.80
+1.20	2400	3.25	0.91	3400	700	0.80
+1.30	2620	2.80	0.91	3800	1000	0.80

potential, associated with a decrease of the corresponding relaxation frequencies f_{max}. These become nearly constant for passive layers, preformed at +1.40V, and measured at +1.00V to +1.30V. C_{HF} values are rather low, being few $\mu F/cm^2$ for the passive layers just formed at +0.300V and +0.325V, and about 15 $\mu F/cm^2$ for the passive layers previously formed. The results are qualitatively very similar to those obtained on pure, polycrystalline Fe[21,36], but with a considerably lower resistance and f_{max} values.

From higher impedances and, in particular, from lower capacitance values, if related to the dissolution, it may be stated that there is a dominance of film capacitance, C_f, which is observed in the total electrode response at high frequencies, just as it was stated for pure Fe.[36] If a passive film is treated as a dielectric, its capacitance per unit area is $C_f = \varepsilon\varepsilon_o/d$, where ε_o is the permittivity of free space, ε the dielectric constant of the passive film, and d is the thickness of dielectric layer. For d varying linearly with potential, there must be a corresponding linear increase of $1/C_f$ with anodic potential.[20,37] This is confirmed by $1/C_{HF}$ *vs.* potential dependence drawn in Figure 7.

In the first approximation, the values of R_{HF} may be considered as the sum of charge transfer resistances on both metal/film and film/solution interfaces and of the resistance of the film, R_f. R_{HF} values increase linearly with anodic potential (Figure 7) and since the current is potential independent, R_{HF} values are not related to the charge transfer resistances. It seems that R_{HF} is mainly under the influence of the film resistance, and that the kinetic effects are masked. The high-field ion migration without influence of diffusion was reported as the origin of R_{HF} for pure Fe[21], and this may also be the case here. The process within the film is rate determining at all potentials within the passive range. As the anodic potential is increased, a constant passive current is ensured by the increase of the layer thickness. For previously formed passive layers, both $1/C_{HF}$ and R_{HF} in dependence on anodic potential are completely in agreement with the predicted dependences for dielectric of defined structure. In terms of the semiconductor band model, the outer part of the passive layer is treated as a dielectric, and R_f and C_f are equivalent to the resistance and capacitance of the space charge.[37]

The low-frequency inductive behavior may be ascribed to the film/solution interface process, as it was shown for the aluminium barrier oxide film.[38] According to the Armstrong and Edmondson[39], the inductive behavior is caused by different responses of the rates of dissolution and formation of the outer layer of passive film on the variation of E.

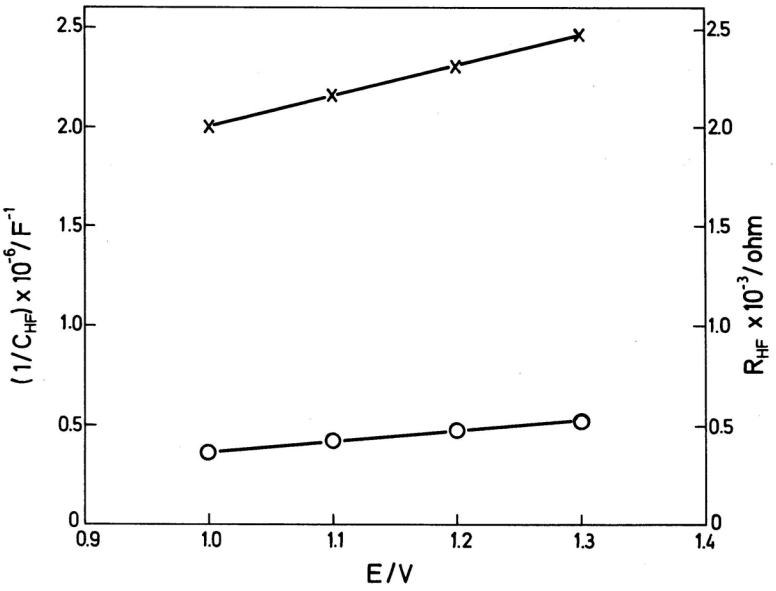

Figure 7. $1/C_{HF}$ (o) and R_{HF} (x) *vs.* E (*vs.* SCE) for the $Fe_{80}B_{20}$ electrode passivated in 1.0 mol dm^{-3} H_2SO_4 at +1.40V.

Here, because of constant passive current, R_p should be constant or even infinite, with anodic potential, due to the infinite slope of the polarization curve in Figure 1. From R_p values listed in Table V, it appears, however, that R_p values increase with ascending potential at the same rate as R_{HF} values increase, which indicates that the origin of inductive loop may be ascribed to some process in the film. Like in the case of Fe, the existence of a slow process may be ascribed to the intermediate oxidation step in the film[21], or to the buildup of surface charge at the metal-oxide interface.[40]

CONCLUSIONS

The steady state polarization curve of glassy metal $Fe_{80}B_{20}$ in 1.0 mol dm^{-3} H_2SO_4 has revealed active-passive transition, with the active dissolution range between –0.480 V and –0.250 V, the passivation or transition range between –0.250 V and +0.275 V and the full passive range extending to about 1V, with a relatively high passive current density.

In the active range, the $Fe_{80}B_{20}$/solution interface impedance dominates the total electrode response. The overall process is a kinetically controlled charge transfer, involving adsorption of intermediate species.

Initial passivation was observed at low frequencies as characteristic capacitative impedance. It becomes the most prominent impedance as the anodic potential increases. The passivation process is mediated by adsorption of some passivating species, which blocks the surface from further dissolution.

Impedance measurements of passive $Fe_{80}B_{20}$ point to the dominance of the passive layer impedance in the overall electrode response. There is indication of a contribution

of surface states relaxation. The rate determining step of the overall electrode reaction is the electric field induced ion-migration. A constant passive current with ascending potential is maintained by the rise in the thickness of the passive layer.

All the results obtained are in general agreement with the data obtained on pure, polycrystalline Fe. This indicates the same overall reaction mechanism of corrosion of $Fe_{80}B_{20}$ and minor influence of B in the active dissolution and passivation or transition regions of anodic potentials, as obvious from minor differences in characteristic impedance parameters. The only identifiable differences are in the increased C_{dl} values, which points to a fast, parallel boron dissolution reaction. However, in the passive range, there is a significant impact of B affecting the chemistry of passive layer. The increased rate of ion transfer reaction (passive dissolution) leads to the degraded properties of the passive layer formed on $Fe_{80}B_{20}$ in 1.0 mol dm^{-3} H_2SO_4 against corrosion.

Acknowledgements. – The authors are indebted to Dr. Mary D. Archer (formerly of the Department of Physical Chemistry, University of Cambridge), and Prof. E. Babić (Institute of Physics, University of Zagreb), for kindly supplying the $Fe_{80}B_{20}$ amorphous glassy ribbons used in this work.

This work has been supported partly through Research Contract No. 5092/RB and Technical Assistance Grant No. 4.023 of the International Atomic Energy Agency, Vienna. The support of the Authority of Scientific Research of the Republic of Croatia, Project No. 1-07-162, and of the Yugoslav Federal Secretariat for Development, Project No. P-96 is acknowledged.

REFERENCES

1. R. B. Diegle, N. R. Sorensen, T. Tsurn, and R. M. Latanison in: *Treatise of Material Science and Technology*, (J. C. Schully Ed.), p. 60. Academic Press, New York, 1983.
2. K. Hashimoto, in: *Passivity of Metals and Semiconductors*, (M. Froment Ed.), p. 235, Elsevier, Amsterdam, 1983.
3. *Rapidly Quenched Metals*, (S. Steeb and H. Warlimont, Eds.), Elsevier, New York, 1985.
4. *Proceedings of the Symposium on Corrosion, Electrochemistry and Catalysis of Metallic Glasses*, (B. Diegle and K. Hashimoto, Eds.), p. 1, The Electrochemical Society, Pennington, 1988.
5. D. Huerta and K. E. Heusler, *J. Non-Cryst. Solids* **56** (1983) 261.
6. D. Huerta and K. E. Heusler, in: Proceedings on the Symposium on Corrosion, Electrochemistry and Catalysis of Metallic Glasses (R. B. Diegle and K. Hasdhimoto, Eds.), p. 1, The Electrochemical Society, Pennington, 1988.
7. K. E. Heusler and D. Huerta, *J. Electrochem. Soc.*, **136** (1989) 65.
8. P. Cadet, M. Keddam, and H. Takenouti, *Proceedings on 4th International Conference on Rapidly Quenched Metals*, p. 1447, Sendai, 1981.
9. M. D. Archer, C. C. Corke, and B. H. Harji, *Electrochim. Acta* **32** (1987) 13.
10. H. Viefhaus, R. Moller, and M. Janik-Czachor, *Werkst. Korros.* **39** (1988) 453.
11. S. Kapusta and K. E. Heusler, *Z. Metallkunde* **72** (1981) 785.
12. P. Kovács, J. Farkas, L. Takács, M. Z. Awad, A. Vértes, L. Kiss, and A. Lovas, *J. Electrochem. Soc.* **129** (1982) 695.
13. P. Cadet, M. Keddam, and H. Takenouti in: *Passivity of Metals and Semiconductors* (M. Froment Ed.), p. 311. Elsevier, Amsterdam, 1983.
14. T. P. Moffat, W. F. Flanagan, and B. D. Lichter, *J. Electrochem. Soc* **135**(1988) 2712.
15. M. Janik-Czachor, *Langmuir* **3** (1987) 910.
16. R. Moller, H. Viefhaus, and M. Janik-Czachor, *Werkst. Korros.* **38** (1987) 322.
17. *Proceedings of the Symposium on Transient Techniques in Corrosion Science and Engineering* (W. H. Smyrl, D. D. Macdonald, and W. J. Lorenz, Eds.), The Electrochemical Soc., Pennington, New York, 1989.
18. M. Sluyters-Rehbach and J. H. Sluyters, in: *Electroanalytical Chemistry* (A. J. Bard, Ed.), Vol. 4, p. 1. Marcel Dekker, New York, 1970.

19. J. Hitzig, K. Jüttner, W. J. Lorenz, and W. Paatsch, *Corrosion Sci.*,**24** (1984) 945.
20. I. Epelboin, C. Gabrielli, M. Keddam, and H. Takenouti, in: *Comprehensive Treatise of Electrochemistry* (J. O. M. Bockris, B. E. Conway, and E. Yeager, Eds.), Vol. 4, p. 151. Plenum Press, New York, 1980.
21. M. Keddam, J.-F. Lizee, C,. Pallotta, and H. Takenouti, *J. Electrochem. Soc.* **131** (1984) 2016.
22. D. A. Harrington and B. E. Conway, *Electrochim. Acta* **12** (1987) 1703.
23. Chu-nan Cao, *Electrochim. Acta* **35** (1990) 831, 837.
24. J. R. Macdonald and W. B. Johnson in: *Impedance Spectroscopy* (J. R. Macdonald, Ed.), p. 1. John Wiley, New York, 1987.
25. U. Rammelt and G. Reinhard, *Electrochim. Acta* **35** (1990) 1045.
26. A. L. G. van den Eeden and J. H. Sluyters, *J. Electroanal. Chem.* **171** (1984) 195.
27. I. Epelboin, C. Gabrielli, M. Keddam, J.-C. Lestrade, and H. Takenouti, *J. Electrochem. Soc.* **119** (1972) 1632.
28. I. Epelboin and M. Keddam, *Electrochim. Acta* **17** (1972) 177.
29. I. Epelboin, C. Gabrielli, M. Keddam, and H. Takenouti, *Electrochim. Acta* **20** (1975) 913.
30. I. Epelboin, M. Keddam, and J.-C. Lestrade, *Faraday Discuss. Chem. Soc.* **56** (1973) 264.
31. H. Schweickert, W. J. Lorenz, and H. Freidburg, *J. Electrochem. Soc.*, **127** (1980) 1693.
32. W. J. Lorenz and F. Mansfeld, *Corrosion Sci.* **21** (1981) 647.
33. B. Bechet, I. Epelboin, and M. Keddam, *J. Electroanal. Chem.* **76** (1977) 129.
34. M. Keddam, O. R. Mattos, and H. Takenouti, *J. Electrochem. Soc.* **128** (1981) 257, 266.
35. O. E. Barcia and O. R. Mattos, *Electrochim. Acta* **35** (1990) 1003.
36. B. D. Cahan and Chia-Tien Chen, *J. Electrochem. Soc.* **129** (1982) 474, 400.
37. K. Azumi, T. Ohtsuka, and N. Sato, *Trans. Jpn. Inst. Met.* **27** (1986) 382.
38. J. Bessone, C. Mayer, K. Jüttner, and W. J. Lorenz, *Electrochem. Acta* **28** (1983) 171.
39. R. D. Armstrong and K. Edmondson, *Electrochim. Acta* **18** (1973) 937.
40. H. J. de Witt, C. Wijenberg, and C. Crevecoeur, *J. Electrochem. Soc.* **126** (1979) 779.

SAŽETAK

Impedancija staklastog metala $Fe_{80}B_{20}$ u sumpornoj kiselini

D. Hodko, K. Kvastek, V. Horvat i V. Pravdić

Opisani su rezultati eksperimentalnog istraživanja korozije staklastog metala $Fe_{80}B_{20}$ u 1.0 mol dm^{-3} H_2SO_4. Prikazani su rezultati voltametrijskih i impedancijskih mjerenja u tri karakteristična područja anodnog potencijala. Opažena su najmanje dva relaksacijska procesa koji su identificirani kao: (*i*) kinetički kontrolirani proces prijenosa naboja kroz međufazu, koji se odvija preko adsorpcije intermedijarnih specija u području potencijala aktivnog otapanja; (*ii*) isti proces, ali uz efekt blokiranja površine uslijed adsorpcije pasivizacijske specije u pasivizacijskom ili prijelaznom području potencijala; (*iii*) proces ionske migracije u jakom električnom polju; uz adsorpciju »površinskih stanja« u području potencijala pasivnog stanja. Upotrebom općenitog izraza za impedanciju u slučaju netrenutačne promjene otpora s potencijalom, mjerene su impedancije karakterizirane u terminima parametara odgovarajućih električkih ekvivalentnih krugova.